RESEARCH ARTICLE | DECEMBER 06 2022

Ionization-induced optical heterogeneity and ion-like direct emission in 1-nm silicon nanoparticle grains: Prospect for fast optical modulation

Kevin Mantey; Huw Morgan ; Ammar Nayfeh; Ersin Bahceci ; Munir H. Nayfeh

AIP Advances 12, 125007 (2022)
https://doi.org/10.1063/5.0122366

Ionization-induced optical heterogeneity and ion-like direct emission in 1-nm silicon nanoparticle grains: Prospect for fast optical modulation

Cite as: AIP Advances 12, 125007 (2022); doi: 10.1063/5.0122366
Submitted: 24 August 2022 • Accepted: 4 November 2022 •
Published Online: 6 December 2022

Kevin Mantey,[1] Huw Morgan,[2] Ammar Nayfeh,[3] Ersin Bahceci,[4] and Munir H. Nayfeh[1,a)]

AFFILIATIONS

[1] Department of Physics, University of Illinois at Urbana-Champaign, 1110 W. Green Street, Urbana, Illinois 61801, USA
[2] Department of Physics, Aberystwyth University, Penglais, Aberystwyth, Ceredigion SY23 3BZ, United Kingdom
[3] Electrical Engineering and Computer Science, Khalifa University, Abu Dhabi 127788, United Arab Emirates
[4] Department of Metallurgical and Materials Engineering, Iskenderun Technical University, 31200 Hatay, Turkey

[a)] **Author to whom correspondence should be addressed:** m-nayfeh@illinois.edu

ABSTRACT

Silicon, a highly symmetric and homogeneous material, does not exhibit fast optical modulation. Recent classical electrodynamics simulations, however, demonstrated transient optical heterogeneity in silicon nanostructures, in which a high-density of excitonic electron–hole pair plasma and charge is created. The phenomenon, however, requires a specific particle size (~100 nm diameter) and a high-density (10^{23}/cc) plasma. We examine here the quantum aspect of the heterogeneity in 1-nm Si nanoparticles. Due to the small number of atoms, 1 nm nanoparticles are amenable to the Hartree–Fock first principle atomistic quantum theory simulations procedure, while single ionization events are sufficient to provide high charge density (2×10^{21}/cc). The simulations show that the charge distribution in singly charged 1-nm particles is nonlinear and heterogeneous, accompanied with structural distortion that produces an electric dipole moment. Electronically, the simulations show that the single charge induces stationary Coulomb states that riddle the bandgap of the neutral particle, with dipole-allowed transitions, effectively inducing partial conducting-like behavior. Optically, when the charge is produced by ionizing UV radiation, the ionized particle survives and exhibits both extended (wide-band) as well as atomic- or ion-like sharp emission, in agreement with infrared polarimetry and spectroscopy observations in the solar coronal holes, as well as under synchrotron irradiation. Not only do ionized Si nanoparticles (charged nanosilicon grains) afford fast optical modulations, but they may also prove pivotal for understanding features of interstellar medium, observed throughout the Milky Way and other galaxies, including spectroscopic and material composition, as well as neutral hydrogen abundancy.

I. INTRODUCTION

There is current interest in the development of optics-based signal modulators because optical signals can be conveyed and processed much faster than their electronic counterpart.[1–10] Fast optical modulation requires fast manipulation and control of the symmetry and the heterogeneity of the optical characteristic of the employed material. Because of their reduced interdistances, optical modulators employing nanoscale-based elements afford the highest speed. Moreover, due to their strong plasmonic response, metal nanostructures can efficiently localize and rapidly control light on a small scale and as such are the material of choice. However, the use of metal suffers from appreciable loss due to Joule's heating resulting from strong electron motion. Attention has been turning to the feasibility of developing conditions under which dielectrics or semiconductors, especially silicon, would act as an alternative material to metal. The interest in silicon is based on amenability for optical nonlinearities and two-photon absorption, as well as the

efficiency of photoexcitation of high density of electron–hole pairs (EHP),[11,12] with high damage threshold, high melting temperature (~1690 K), and structural stability. However, due to its centrosymmetry, bulk silicon is a linear crystal with negligible nonlinearity, being zero at the second order level. Moreover, it has very small third order nonlinearity and, therefore, offers no heterogeneity.

Recently, classical theoretical simulations using a finite difference time domain (FDTD)[13,14] of nanostructures showed that, under highly intense fast femto-second laser radiation, silicon, which is otherwise highly symmetrical and homogeneous, exhibits fast manipulation and control of its symmetry and heterogeneity, promising fast optical modulation. The novel dynamic nanoscale effect is characterized by an induced transient electric conductivity and induced heterogeneous refractive index configuration.[1,15] These were attributed to the creation of a high density of charge/plasma (excitons), accompanied with a significant rate of ionization resulting from avalanche, photo, and Auger-recombination ionization.[16] It should be noted that, in addition to the heterogeneous changes (symmetry breaking and magnetic optical resonance tuning),[6] there are transient homogeneous changes in the dielectric permittivity and the refractive index (without any consideration of the asymmetrical distribution of EHP).[8,9] Those may be also used as controlling parameters for light manipulation at the nanoscale.

The heterogeneity is found to be limited, however. First, it requires an intermediate size range of 75–110 nm, for which the optical excitation of the electric and magnetic Mie[17] resonances occurs simultaneously.[18,19] Second, it requires the formation of a heterogeneous high density of EHP plasma charge ($5 \times 10^{21}/cm^3$), which requires excitation with high field intensity ($10^{12}/cm^2$ peak intensity). Such a critical high density[1,12] of charge plasma is a significant fraction of the atomic density of silicon particle saturation density[20] ($5 \times 10^{22}/cm^3$). A heterogeneous distribution of high plasma charge evolves asymmetrically, which provides symmetry breakage as well as a transient metallic behavior in silicon, which is otherwise a non-conducting material. In other words, the nanoparticle acquires a certain degree of heterogeneous metallic properties [Re (ε) < 0], hence, heterogeneous optical constants, which allows manipulation with much reduced Joules heating and losses. Previously, under similar conditions of peak intensity, pulse width, and wavelength, silicon nanoparticles at much reduced size (1-nm), which do not exhibit electric and magnetic scattering resonance in the visible, showed second order nonlinearity and harmonic generation.[21] The effect was attributed to a broken centrosymmetry caused by strong structural surface re-construction that induced strong mechanical strain that lead to several optical nonlinearities.

It would be interesting to conduct a quantum mechanical study of ultrasmall 1-nm silicon nanoparticles with a specific molecular configuration $Si_{29}H_{24}$ that allows "exact" atomistic theory to examine some aspects of the effect of plasma on the optical heterogeneity to discern *or get some hints on* the basic mechanism. 1-nm particles are small enough to be amenable to atomistic quantum mechanical theory simulations, while eliminating the Mie scattering[17] of all types in the visible, which may isolate the effect of the charge. In addition, the charge density corresponding to a single positive charge (single electron) is $1.7 \times 10^{21}/cm^3$, which is a good fraction of the bulk density of silicon ($5 \times 10^{22}/cm^3$). Thus, even a single positive charge in 1-nm particle corresponds to a charge density, which is close to the critical density suggested for the realization of the plasma nonlinearity in the larger 100-nm particles. However, one should note that it is not clear if any result from a 1-nm particle can be directly translated to 100-nm particles. The 1-nm particle is at the edge of the molecular-atomic regime, with only one tetrahedral unit core (24:5 surface to bulk) while a 100-nm particle is at the edge of thee bulk regime. Using the full atomistic quantum mechanical theory in the presence of a single ionization event, we detail in the study the electronic structure and energy levels and bandgap, transition oscillator strength and luminescence spectrum, bond lengths and angles and topographical symmetry, electronic charge distribution, and electric dipole moment. Our results show that a single charge event induces nonlinear heterogeneous charge distribution and structural distortion, accompanied with an electric dipole moment. The bandgap is found to be riddled with 23 induced Coulomb states bunching in five bands with a spacing of ~0.5 eV on the average, and with ~20–40 meV interspacing, effectively reducing the bandgap reflecting some partial conducting-like behavior. The quantum-induced heterogeneity in silicon nanostructures may afford the silicon fast optical modulation functionality. Moreover, charged nanosilicon grains may be useful for understanding features of interstellar medium, including spectroscopic and material composition, as well as neutral hydrogen abundancy.

II. THEORETICAL SIMULATION

A. Wavefunctions and eigenstates

We carried out Hartree–Fock based atomistic calculations of the quantum mechanical wavefunctions and obtained the electronic structure of the neutral 1-nm particle as well as the charged form (single electron stripped from the highest occupied molecular orbital). To facilitate the comparison, we use a specific molecular configuration of a 1-nm particle, namely, $Si_{29}H_{24}$. We employed the Restricted Hartree–Fock (RHF) theory with the 6-311 G (d, p) basis set available in the General Atomic and Molecular Electronic Structure System (GAMESS) quantum chemistry package.[22–24] The 1-nm nanoparticle structure is amenable to such calculations because it consists of a small number of atoms. We examined the electronic structure of the charged particle in which a single electron was stripped from the top of the valence band highest occupied molecular orbital (HOMO), creating a vacancy, or hole state, which results in a half-filled orbital ("half-filled HOMO"). We calculated the excited wave functions and the eigenenergies of the filled valence states lying below it and of the lowest unoccupied molecular orbitals (LUMO) states lying above it. Since the half-filled HOMO ground state does not have a Tetrahedral (TD) symmetry, we searched for states with dipole allowed transitions to the ground states. We summarize in the partial energy diagram given in Fig. 1(a) the states of symmetry such that they have dipole-allowed transition to the ground state. The transitions have a wide range of the oscillator strengths spanning a range over several orders of magnitude from 10^{-2} to 10^{-7}, which corresponds to more than ten-orders of magnitude variation in the cross-section, approaching those of forbidden states. In addition, for comparison, we give in Fig. 1(b) parallel calculations of the energy level diagram of the neutral particle. The electronic structure in the proximity of the HOMO–LUMO gap shows several interesting features in the charged particle. We see the introduction of a manifold of about 50 states within the HOMO–LUMO gap of the neutral particle. The

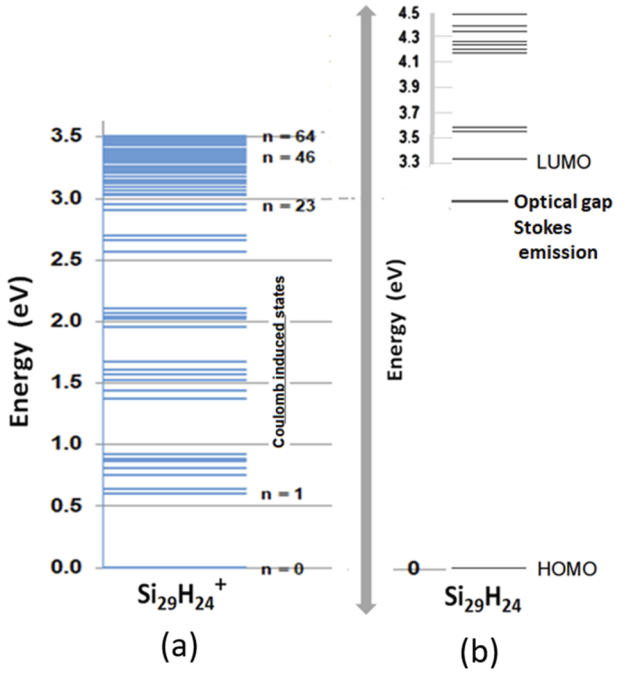

FIG. 1. Calculated partial energy diagram of neutral $Si_{29}H_{24}$ and ionized $Si_{29}H_{24}{}^{+1}$ particles in the proximity of the HOMO–LUMO bandgap. (a) Eigenelectronic states of the ionized particle lying just below the edge of the bandgap of the neutral particle and of the states lying above it (empty states above gap or "conduction/continuum" states) (0–3.7 eV). (b) Eigenelectronic states of the neutral particle (0–4.6 eV) for comparison.

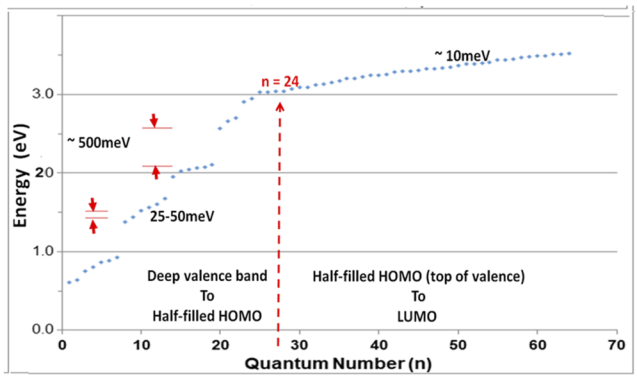

FIG. 2. "Coulomb induced states" of $Si_{29}H_{24}{}^{+1}$ detailing the energy E and the quantum number n of the 64 states. 46 states within the HOMO–LUMO gap of the neutral particle. The states are ~20–50 meV apart and exhibit several breaks or "gaps" of about 0.5 eV. The states pile up as they cross 3.32 eV, the LUMO limit of the neutral. We plotted the first 18 (~10 meV apart) higher states that lie above 3.32 eV. For $n < 24$ states, contributions are mostly valence to valence, from filled valence band orbitals to the half-filled orbital at the top of the valence band. For $n > 24$ states, contributions are mostly valence to conduction, from top of the valence band state (half-filled HOMO) to empty conduction states above the gap.

states are not equally spaced and exhibit several breaks or "gaps." The lowest excited state in the discrete manifold lies 0.6 eV above the HOMO state, which is the largest gap. The states pile up as they cross 3.32 eV, which is the LUMO limit of the neutral. The lowest lying ones are ~0.10 eV apart on the average corresponding to an average wavelength of ~12 μm. The manifold has 46 discrete states within the HOMO–LUMO gap of the neutral (the energy range is 0.0–3.32 eV), while there are more than 18 higher states that lie above 3.32 eV.

The discrete states are "Coulomb induced" states, which are due to the Coulomb breakage of symmetries allowing more transition to become dipole allowed. This indicates that the charging (Coulomb effect) provides a rich spectrum of narrow lines in the near infrared. Contrary to transitions in the neutral particle, which are wide molecular-like bands, the Coulomb induced lines are more-like atomic discrete direct lines, which are reasonably narrow. Although the two holes and electrons in an excited particles may be looked at as an X^+ trion or $H2^+$-system, the structure may not actually be bound since the ultrasmall nanoparticles create a very strong confinement conditions in which the two holes are not bound and that the three charges are unbound or quantum mechanically independent of each other.

It is interesting to discuss some other features of the "Coulomb induced states" of $Si_{29}H_{24}{}^{+1}$ with the aid of Fig. 2. First, the 64 excited states are more-like discrete states, but as we cross 3–0 eV, we find that the states stay discrete but they start to pile up just like in a continuum band (10 meV spacing). The first lowest 24 states (1–24) are transitions from filled valence band orbitals to the half-filled orbital at the top of the valence band or what is called the LUMO state. For states above 3 eV, transitions begin to contribute from the top of the valence band state (half-filled HOMO) to states above the gap. It is to be noted that we find no pure cutoff between both regions in terms of the origin of the transitions, namely, transitions to the half-filled orbital, vs transitions to empty orbitals (above "the gap"). The 25 state is the first one to start having sizable contributions from transitions above gap energy = 3.028 658 395 319 102 eV. State 29 lasts to still have large contributions from the full tilled states → half-filled that is greater than 10% energy = 3.066 082 201 435 870 eV. In addition, state 30 and on, transitions are almost completely from the half-filled state to empty orbitals (i.e., above gap) energy = 3.089 902 287 605 444 eV. The 64 state is the last calculated energy = 3.521 537 776 793 876 eV. Since the states that start to involve "gap transitions" are at 3 eV, we define the bandgap edge in the ionized particle to be at 3.0 eV. This energy is close to the Stokes shifted optical gap in the neutral particle.

For comparison, we also give on the right of Fig. 1(b) the relevant energy edges of the neutral particle: the HOMO and LUMO edges at zero and 3.32 eV as well as the Stokes shifted edge at which the luminescence proceeds (optical gap edge at 3.0 eV).[25,26] In addition, we show the lowest ten discrete excited states above the LUMO state. Those are embedded in the conduction band. They can be organized in three bands (3.29, 3.5, 3.55), (4.1687, 4.196, 4.2318, 4.2606), and (4.3401, 4.3802, 4.483). As one can see, upon ionization, the bandgap gets riddled with discrete levels. The lowest lying 23 induced coulomb states bunch up in four sets with a spacing of ~0.5 eV on the average. Within each band, the spacing is within room-temperature thermal energy (~20–40 meV), while states above the 3.0 edge are sub room-temperature thermal energy (10 meV) apart.

B. Oscillator strength-atomic-like transitions

The oscillator strength of the optical transitions to the ground state in the charged particle was obtained from the calculated wave functions and is plotted in Fig. 3(a) along with the energy and the quantum number of the respective states. We also present the oscillator strengths of the neutral particle, shown in Fig. 3(b), along with the energy of those states.[25,26] The neutral particle has a TD symmetry, making all transitions dipole forbidden, in those calculations. However, during absorption, the TD symmetry is broken due to the resulting inflation of a component of the particle, i.e., stretching of one of the dimer-like bonds due to absorption-induced mechanical strain. The inflation of a dimer-like bond automatically occurs in the absorption and emission processes. On the other hand, many transitions in the stripped particle are electric dipole allowed without a need for inflation. Creating a positive charge by ionizing an electron breaks the symmetry. This implies that the ionized particle does not have a TD symmetry. Since the $Si_{29}H_{24}$ structure has a Td point group symmetry, this high symmetry makes many of the electronic states degenerate. When the structure is broken to C2v symmetry by stretching the dimer, the B2 states will arise from Td representations splitting into C2v representations as follows: T1 → A2 + B1 + B2 and T2 → A1 + B1 + B2. Only T2 representations are dipole allowed, so the lowest B2 excited state, which originates from T1, is not even dipole allowed.

The oscillator strength in the stripped particle is found to concentrate in a few transitions. For instance, the transition from state 23 to the ground state, at an energy of 2.9 eV, has a value of 0.8×10^{-2}. In addition, level 27 at 3.03 eV has an oscillator strength of 0.16×10^{-2}. The energies line up with the Stoke shifted emission edge of the neutral particle (optical band edge) at 3 eV. Therefore, we associate the 23-energy state (2.9 eV) with an edge for optical emission (optical bandgap) in the ionized particle. Transitions from some levels lying in the middle of the gap around level ten at 1.53 eV with an oscillator strength of 1.09×10^{-2} pile up in the infrared to produce a band at ~ 810 nm. A group of about ten levels (54–64) may lead to a UV band at ~3.5 eV. The corresponding oscillator strength is much smaller for all higher lying states including those near the 3.32 eV edge. Thus, de-excitation by showering though the Coulomb states, which results in deep infrared radiation, is much slower than the optical transition from near 2.9 to the HOMO edge.

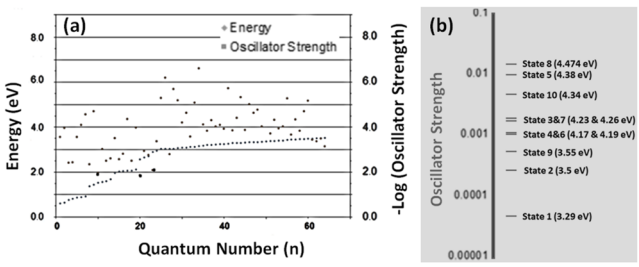

FIG. 3. Oscillator strength of the optical transitions from the Coulomb induced states to the ground state (a) in the charged particle plotted against the energy and the quantum number of the respective induced states and (b) in the neutral particle along with the energy of the states.

C. Luminescence

The luminescence spectrum of the ion can now be calculated after an exciton has been excited to a high lying state from the oscillator strengths and the transition energies (see Table I). The "emission" is made by taking the emission at each wavelength to be proportional to "oscillator strength"/wavelength^2 ~ f/λ^2 (i.e., the emission strength is proportional to the transition rate of that energy level to the ground state). The emission that dominates the luminescence is shown in Fig. 4. The emission may be organized into four bands: near ultraviolet, blue, red and infrared, and deep infrared bands. As expected from first principal calculations, each band appears as discrete lines, but accounting for finite temperature widths, and other broadening effects turn them into more like continuous bands. In the spectrum shown, we applied a 5 nm Gaussian width to each line. The ultraviolet (UV)/blue band (340–500 nm) carries ~70%. The red band (~600–850 nm) carries 29% while the deep infrared (1533–1638 nm and 2.5–50 μm) carries only 1%–2%. The blue/red/infrared luminescence bands originate from transitions equivalent to state hopping of a single hole within the valence band, and the near UV band originates from recombination. All other transitions from the induced manifold to the HOMO or between the induced states are found to be weak transitions because of much smaller oscillator strength or/and longer emission wavelength in the infrared.

The de-excitation by showering though the Coulomb states, which results in deep infrared radiation, is still much slower than the optical transition from near 2.9 to the HOMO edge. In other words, the rate of energy loss to heat due to Coulomb scattering is not significant. This explains why the luminescence is significantly reduced but not completely quenched for excitation as high as 22 eV, the range studied in this report. It is be noted that 2.9 eV matches the Stokes shifted edge for emission in the neutral particle. Moreover, the strength of this transition is comparable to that of the Stokes shifted emission in the neutral particle. This may explain why the blue spectrum of the neutral particle does not change significantly when excited by ionizing radiation. Finally, this is consistent with the fact that, in particles, which are considerably smaller than the size of the exciton (4.3 nm), the confinement is very strong, which weakens electron–hole coupling, rendering each to move independently.[27,28]

Measurement of the vibration modes of the 1 nm particle showed evidence of diminishment of the bulk-like vibration in favor of molecular-like vibration that is confined mostly to the outer bonds in the particle.[29] This may allow electron–electron scattering in the molecule-like system to dominate, enabling conversion of the excess energy to electronic excitation.

D. Charge and structural heterogeneity

We examined the effect of ionization on the geometry of the particle in its ground state. We computed the equilibrium coordinates of the Si atoms before and after ionization and obtained changes in positions of the atoms as well as in the bond lengths and angles. We now present in Fig. 5 the electronic charge distribution of outer electrons in the ground state of the charged particle ($Si_{29}H_{24}^{+}$) and contrast it with that of the neutral particle ($Si_{29}H_{24}$). The distributions are calculated from the calculated wave function of the ground state. Figure 5(a) presents the neutral particle case with red

TABLE I. Exciton oscillator strengths and transition energy data.

Excited state	Energy	Oscillator strength		Excited state	Energy	Oscillator strength	
1	0.604 776 344	2.75×10^{-4}	3.560 359 941	33	3.129 306 688	8.32×10^{-6}	5.079 932 566
2	0.640 481 992	1.11×10^{-4}	3.954 124 934	34	3.152 563 336	2.46×10^{-7}	6.609 606 585
3	0.756 432 045	3.85×10^{-3}	2.414 009 031	35	3.176 854 234	7.59×10^{-5}	4.119 636 222
4	0.808 458 517	3.73×10^{-3}	2.428 434 423	36	3.205 458 903	1.44×10^{-4}	3.841 132 951
5	0 864 501 483	2.77×10^{-4}	3.556 860 757	37	3.205 563 575	4.95×10^{-5}	4.305 439 388
6	0.889 894 613	8.05×10^{-5}	4.093 951 9	38	3.224 496 399	9.46×10^{-5}	4.024 032 627
7	0.924 141 816	2.73×10^{-5}	4.563 816 01	39	3.245 042 785	7.93×10^{-5}	4 100 692 497
8	1.374 201 627	4.49×10^{-3}	2.347 821 311	40	3.246 261 128	1.22×10^{-4}	3.913 458 117
9	1.440 238 943	1.99×10^{-5}	4.701 017 109	41	3.259 165 956	1.91×10^{-6}	5.718 855 01
10	1.526 851 817	1.09×10^{-2}	1.961 392 452	42	3.290 334 759	1.41×10^{-4}	3.852 222 651
11	1.568 032 826	9.70×10^{-4}	3.013 367 727	43	3.295 973 858	3.88×10^{-5}	4.411 264 838
12	1.604 947 363	3.11×10^{-3}	2.506 757 054	44	3.299 650 701	4.80×10^{-6}	5.319 197 297
13	1.677 526 827	2.50×10^{-3}	2.602 870 454	45	3.310 865 298	1.35×10^{-4}	3.868 768 37
14	1.953 605 6	3.16×10^{-4}	3.500 097 921	46	3.326 079 947	9.54×10^{-6}	5.020 256 645
15	2.026 799 241	2.72×10^{-3}	2.565 907 625	47	3.326 259 217	2.37×10^{-5}	4.624 605 804
16	2.045 035 893	1.53×10^{-3}	2.815 542 833	48	3.339 005 117	1.71×10^{-5}	4.768 199 142
17	2.068 763 66	4.39×10^{-5}	4.357 091 609	49	3.345 890 703	9.57×10^{-5}	4.019 190 925
18	2.072 567 087	3.12×10^{-3}	2.506 196 267	50	3.364 418 019	4.98×10^{-9}	8.302 388 697
19	2.110 719 17	1.07×10^{-4}	3.970 987 03	51	3.387 393 027	1.95×10^{-4}	3.709 337 845
20	2.571 777 483	1.38×10^{-2}	1.859 209 629	52	3.389 775 674	4.77×10^{-5}	4.321 050 471
21	2.657 768 122	1.16×10^{-3}	2.934 900 318	53	3.394 667 818	1.16×10^{-4}	3.935 934 015
22	2.701 159 999	1.72×10^{-3}	2.765 438 381	54	3.405 859 997	9.54×10^{-5}	4.020 349 169
23	2.904 922 249	8.14×10^{-3}	2.089 463 483	55	3.435 600 772	5.29×10^{-6}	5.276 770 893
24	2.950 057 706	4.27×10^{-4}	3.369 217 188	56	3.445 281 43	2.22×10^{-4}	3.654 274 368
25	3.028 658 395	5.16×10^{-6}	5.287 426 886	57	3.449 750 531	4.66×10^{-5}	4.331 409 569
26	3.034 458 718	6.52×10^{-7}	6.185 580 8	58	3.473 273 228	1.46×10^{-4}	3.836 594 424
27	3.036 383 768	1.57×10^{-3}	2.802 747 666	59	3.479 228 092	2.01×10^{-5}	4.697 149 458
28	3.042 125 888	2.03×10^{-6}	5.692 009 042	60	3.496 202 754	6.84×10^{-6}	5.164 782 18
29	3.066 082 201	6.39×10^{-6}	5.194 414 804	61	3.496 612 114	3.59×10^{-4}	3.444 585 091
30	3.089 902 288	6.30×10^{-5}	4.200 781 11	62	3.510 949 439	4.29×10^{-4}	3.367 951 684
31	3.091 134 876	2.35×10^{-5}	4.628 867 262	63	3.511 685 24	3.27×10^{-4}	3.485 093 909
32	3.121 828 37	2.67×10^{-4}	3.573 691 168	64	3.521 537 777	7.23×10^{-4}	3.141 104 252

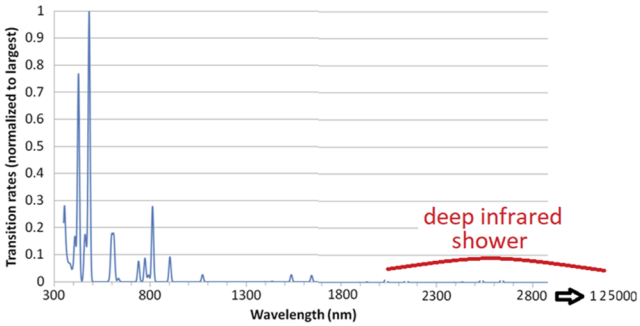

FIG. 4. Estimated calculated luminescence spectrum of the ion after an exciton has been excited, using the oscillator strength f and the transition wavelength λ (~"osc strength"/wavelength^2 ~ f/λ^2). The emission is organized into four bands: near ultraviolet, blue, red and infrared, and deep infrared bands. A 5 nm Gaussian width has been applied to each line.

and blue and yellow distributions illustrating the electron density of the degenerate highest occupied molecular orbitals. The electronic charge distribution is uniformly distributed, with the particles having no dipole moment. Figure 5(b) presents the positively charged particle in which the degeneracy is broken. The order of energy is the fully filled orbital in yellow and blue, then the half-filled orbital in red. The electronic charge distribution in the charged particle is not uniformly distributed, having a permanent dipole moment. Figure 5(c) presents the electronic charge distribution of the charged particle with an arrow indicating the direction of the dipole moment.

The dipole moment is significant, being ~2.5 D with the center of electron charge being displaced from the center of the positive charge by ~1.25 A. We correlated the charge distribution with the shape of the particle. We computed the equilibrium coordinates of the Si atoms before and after ionization. Very little change is found in the bond lengths, but bond angles change. The change is very little in the bond lengths in two directions. In one direction,

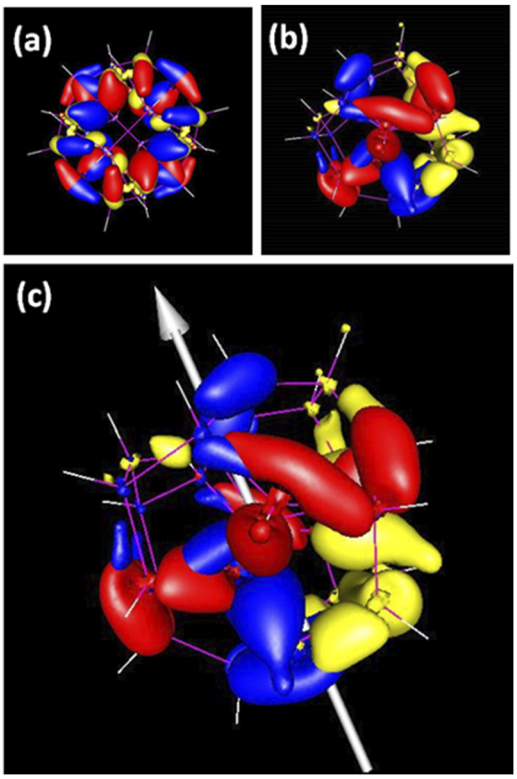

FIG. 5. Electronic charge distribution in the ground state of the charged particle ($Si_{29}H_{24}^{+1}$) and contrast it with that of the neutral particle ($Si_{29}H_{24}$). The distributions are obtained from the calculated wave function of the ground state in each case. (a) The neutral particle case with red and blue and yellow distributions illustrating the electron density of the degenerate highest occupied molecular orbitals. The electronic charge distribution is uniformly distributed, with the particles having no dipole moment. (b) Positively charged particle with the degeneracy broken. The order of energy is the fully filled orbital in yellow and blue, then the half-filled orbital in red. The electronic charge distribution in the charged particle is not uniformly distributed, with the stripped particle having a permanent dipole moment. (c) The electronic charge distribution of the charged particle with an arrow indicating the direction of the dipole moment. In the electric dipole direction, the particle swells by ~0.08 Å, making the particle non-spherical.

however, the particle swells by ~0.08 A, causing asymmetry and making the particle non-spherical, with the electric dipole direction being in the direction of swelling. In other words, the direction of the dipole moment in the stripped particle is along the axis of elongation.

It has been known or assumed that, in large, charged clusters, the charge distribution is uniformly distributed, with the particles having no dipole moment. The present results confirm using the calculated wave function of the ground state that the charge in nano-sized 1 nm charged-particles is not uniformly distributed, with the particle having a permanent dipole moment. The quantum asymmetry found in the ultrasmall particles of 1-nm diameter is consistent with the classical symmetry reported in 75–100 nm particles,[1,15] but it is not clear if the origin is the same.

III. EXPERIMENTS ON ABOVE IONIZATION THRESHOLD LUMINESCENCE-IONIZING RADIATION

We used electrochemical etching in a mixture of HF and H_2O_2 to disperse crystalline Si wafers into ultrasmall nanoparticles.[30–34] The wafer was laterally etched to concentrate the etching current on the surface. The procedure forms on the surface a set of discrete sizes of 1, 1.67, 2.2, and 2.9 nm diameter particles. The treated wafer was then transferred to an ultrasound bath using a liquid of choice, producing a soup (mixture) of the sizes. Because the particles are ultrasmall (<3 nm in diameter), they dislodge under sonification into a stable colloidal suspension. The oxidative nature of the peroxide produces chemically and electronically high-quality samples with good passivation. The particles are hydrogen passivated with a monohydride (Si–H). The nanoparticle suspension can be stored for later use for an extended period under ambient temperature. High-resolution TEM shows that, under certain conditions, the procedure produces a family of discrete, nearly spherical, nanoparticles.[35–37] To prepare thin-film samples on silicon wafers starting from the suspension, we use one of several procedures including electric spray, atomization, incubation, or simple drop evaporation. As to the size distribution, samples prepared under high-current etching tend to produce smaller particles and are usually dominated by one size (1-nm particles), with a small percentage of contamination from other sizes. Under lower currents, the procedure produces red luminescent nanoparticles with 85% purity and the remaining are other sizes, because high etching current injects high-density of hole, and hence a high etching rate.

It is interesting and useful to discuss the storage time (shelf time) of the nanoparticles and their effect on the optical properties due to changes in the particle surface condition or terminated functional groups. Particles of different sizes have been stored in a variety of liquids including water, alcohol, benzene, and THF.[32–34,38] The monohydride Si–H tends to be very stable and highly inert against interactions such that 3-nm particles can be stored in alcohols for several years without much change to their optical emission. In water solvents, however, they tend to agglomerate and precipitate because H-passivated silicon surfaces are hydrophobic. For particles that are functionalized with acid groups on the surface, the solubility of the modified particles is sensitive to the pH of the solvent. For example, aggregation was observed upon lowering of the pH of the water colloid to pH < 5. However, increasing the pH to the original value restored its transparency. HCl interacts with carboxylate particles in basic water solution if there are residual Si–H (incomplete functionalization) groups. After keeping the aqueous sample with pH = 2 for two months, its PL was completely quenched. The sample hydrolyzed under softer acidic conditions (starting pH equal to 4.9 and self-increased up to seven at the end of the experiment), as well as lost the PL after five months.[32–34,38]

We examined in detail the effect of pH environment on the stability of the luminescence and dispersion of Si–H terminated Si nanoparticles.[32–34,38] The measurements show that the buffer quenches the luminescence. In the measurements, we recorded the luminescence of a colloid of monodispersed Si nanoparticles as a function of the volume of the buffer added. The buffer used is a diluted with water pH 10 mixture of potassium carbonate, potassium borate, and potassium hydroxide buffer. Since the Si nanoparticles are synthesized with a Si–H termination, we believe that the buffer deprotonates the particles resulting in a radical (Si–H, Si–), which

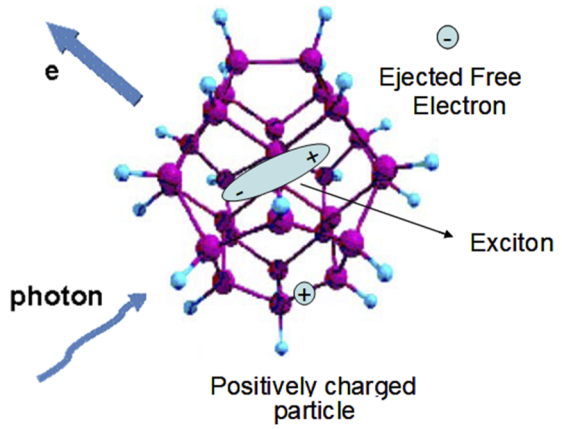

FIG. 6. Schematic of the X^+ positive trion in a silicon nanoparticle of 1 nm diameter. The system consists of two holes and one electron. The trion is formed by stripping an electron from the particle to the surrounding region leaving behind a positive charge (hole). The stripping may take place by photons or charged particles. This is followed by the creation of an exciton consisting of an electron and a hole (electron–hole pair) using photon or electron excitation. The two processes may take place sequentially or simultaneously by a single or two events.

makes them highly reactive with the environment, in turn resulting in surface traps that quench the luminescence. On the other hand, measurements show that acids such as HCl do not quench the luminescence of the pure Si nanoparticles. In fact, upon adding 1 M HCl to Si nanoparticles colloid in isopropanol, resulting in a pH drop from 6.5 to 1, the average brightness was measured at a level of 210 arbitrary counts compared to the initial brightness of 200 (luminescence images not shown). The stability is because HCl maintains the hydrogen termination of the particles. 1-nm blue luminescent particles are unlike 3-nm particles, which have only one tetrahedral unit core, and they are more polarizable and have a significant Mullikan charge at the Si–H surface bond. They form stable colloids in water, but they are eventually dissolvable in water over several months to produce molecular compounds. They can also be stored in a variety of other liquids including alcohol, benzene, and THF.

The response of monodispersed 1-nm silicon nanoparticles to ionizing ultraviolet (VUV) excitation energies covering the range of 4.5 to 22 eV was studied by synchrotron radiation.The non-bake base pressure is 10^{-8} Torr at room temperature and $<10^{-10}$ Torr at 10° K.[39] The measurement system covers the photon energy range of 5–35 eV (2500–350 Å) and a resolution of 0.05 Å. The detection uses GaAs-based photocathode tubes (GaAs and GaInAs:Ce).

The silicon nanoparticle is stripped using photoionization as cartooned in Fig. 6. We note that the photoionization energy for bulk silicon is in the range of 4.7–4.9 eV, while for isolated single silicon atoms is 8.15 eV. Due to quantum confinement, the photoionization energy in miniaturized particles depends on the size as well as on the surface condition or termination. The photoionization of a 1-nm particle was set at 7.8 eV by several theoretical procedures, including time dependent local density theory (TDLDT)[40–43] and first principal calculations using local-density approximations (LDA) theory.[44–47] Moreover, when the surface is terminated with hydrogen, a second photoionization limit from the hydrogenated

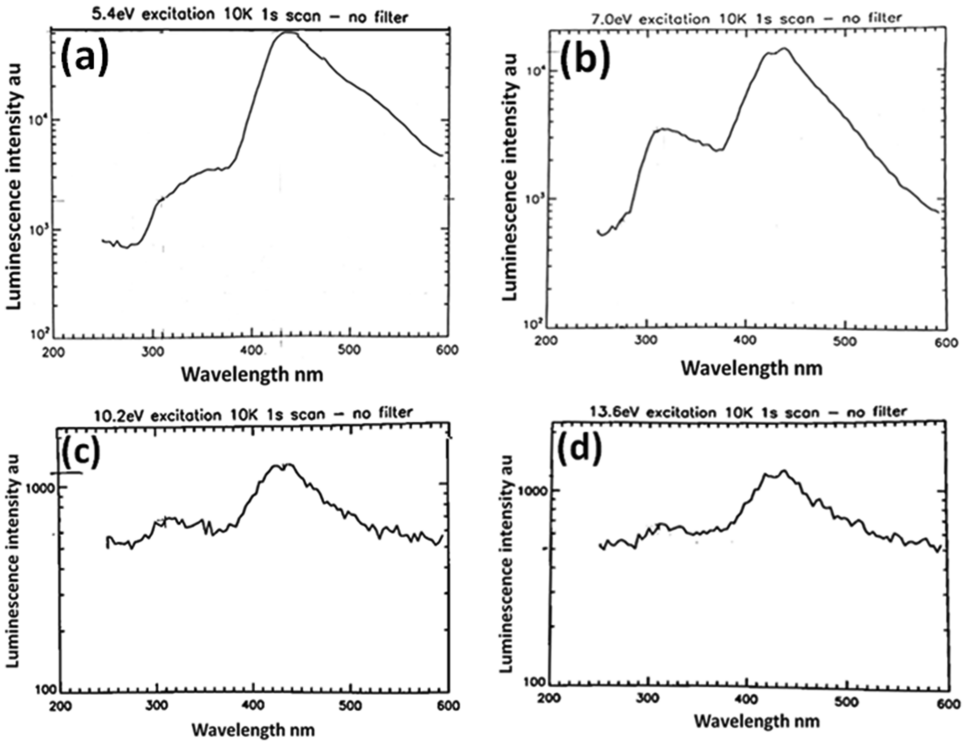

FIG. 7. Emission spectrum over the wavelength range of 250–650 nm of 1-nm particle under excitation in the range of 5–13.6 eV: (a) 5.4 eV, (b) 7 eV, (c) 10.2 eV, and (d) 13.6 eV. The sample is cooled to 10° K. The spectra were corrected for the detector sensitivity.

surface layer (shell) is set by TDDFT at ~9.15 eV[40] and by Feynman–Dyson propagator formalism at ~9.5 eV.[48]

We measured the emission spectrum in the range of 5–12.5 eV. The measurement over this range contrasts the luminescence in two regimes of incident photon energy, namely, smaller and larger than the photoionization energy of the particles. We present in Figs. 7(a)–7(d) some representative photoluminescence spectra below and above the ionization limits, namely, at excitation energies of 5.4, 7, 10.2, and 13.6 eV over the wavelength range of 250–650 nm, with the sample cooled to 10° K. The spectra were corrected for the detector sensitivity. The response at 5.4 eV shows a wide UV luminescence band in the range of 265–350 nm (when resolved, it consists of wide overlapping bands at 265, 310, and 350 nm). The visible band in the blue, which peaks at 425 nm, commences at 390 nm and has a tail out to 500 nm. It is the lowest lying luminescence band that has been measured for the 1-nm particles. This multiple-emission band feature is akin to a cascade emission from excited molecules. Figure 7 shows that the quantum efficiency has dropped by near a factor of 150 for excitation at 13.6 eV compared to excitation at 5.4 eV. However, the spectral distribution has suffered much less change.

The measurements given in Figs. 7(c) and 7(d) show that the particles under ionizing radiation exhibit a blue band luminescence as well as a near UV band luminescence. The branching ratio and position of the calculated bands are in reasonable agreement with the measured spectrum. Although of different origins, the proximity of the size of the optical gaps in the neutral and in the stripped particles indicates that the UV/blue spectrum of the neutral particle does not shift significantly when the particle is ionized. It is plausible that for a photon energy above 9.25 eV, the process involves the ionization of a single electron while the balance of energy results in the excitation of an exciton as shown in Fig. 6. The fact that the 1-nm particles remain bright under ionizing radiation points to the importance of electron–electron or electron–phonon interactions as well as Coulomb scattering. The results lead us to conjecture that in ultrasmall crystals, such as 1-nm particles, the strength of phonon and Coulomb scattering is diminished.[49,50]

IV. DISCUSSION: ATOMIC ION-LIKE LINES

It is interesting to discuss the prospect for induced infrared activity of the ionized nanoparticle. The infrared activity of interest is due to the cascade shower transitions between the Coulomb-induced manifold. We give in Fig. 8(a) an example transition, 35–15, i.e., emanating from state 35, lying at the calculated energy of 3.176 854 eV, to state 15 at 2.026 799 eV. High lying states including 35 have small oscillator strength to the ground state, indicating mixed symmetries. The transition from 35 to 15, for example, may proceed since the direct emission from 35 to the ground state has a very small oscillator strength. Transition to state 15 gives an infrared photon with energy of emission (3.176 854–2.026 799 eV) = 1.150 055 eV, corresponding to a photon of wavelength 1077.3 nm. This transition may be followed by direct transition to the ground state with a sizable oscillator strength to the ground state. Figure 8(b) shows some other nearby transitions. They include transitions 34–14, 39–18, 36/37–16, 38–17, 38–18, 35–15, and 35–16 giving photon wavelengths of 1033.1, 1056.7, 1067.7, 1072.1, 1075.6, 1077.3, and 1094.7 nm, respectively.

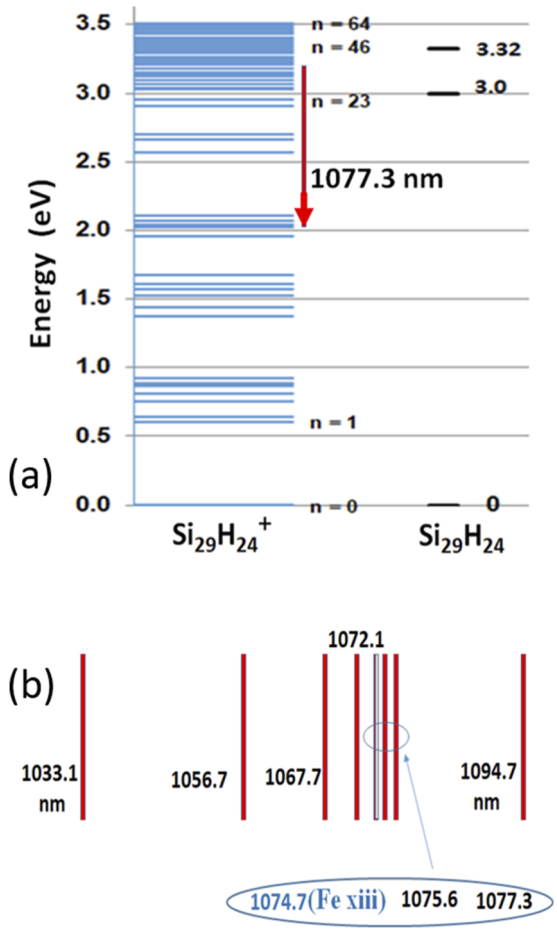

FIG. 8. Wavelength of cascade shower transitions between the Coulomb-induced manifold (a) example transition, 35–15, i.e., emanating from state 35, lying at the calculated energy of 3.176 854 eV, to state 15 at 2.026 799 eV, giving an infrared photon with energy of emission (3.176 854–2.026 799 eV) = 1.150 055 eV, corresponding to a wavelength of 1077.3 nm. This transition may be followed by direct transition to the ground state with a sizable oscillator strength to the ground state. (b) Examples of transitions from high lying states to near mid gap states 34–14, 39–18, 36/37–16, 38–17, 38–18, 35–15, and 35–16 giving photon wavelengths of 1033.1, 1056.7, 1067.7, 1072.1, 1075.6, 1077.3, and 1094.7 nm, respectively.

It is interesting to discuss the infrared activity in relation to infrared polarimetric observations in the solar corona during solar eclipses. Polarization measurements are made by imaging in spectral lines representing different ionization states of iron, sulfur, silicon, hydrogen, and helium, covering blue, red, infrared, and far-infrared parts of the spectrum. One interesting region is the Fe xiii line at 1074.7 nm. The polarimetric observations were made within a 0.58 nm bandpass centered at 1074.7 nm. To observe weak spectra, measurements were made during the total solar eclipse (2001 June 21).[51–53] Moreover, imaging was made in the coronal holes, in the radial extension, starting from the solar surface where

the Fe xiii emission is substantially reduced or absent. Polarimetric observations previously provided a striking marker for the radial extension of coronal hole boundaries as first detected in radio ranging measurements.[54] Our polarimetric observations of the eclipse suggest that there could exist a rich coronal spectrum of narrow lines in the near infrared of a different origin. The measurement targets a tangentially polarized emission in the radial extension of the low-temperature and low-density coronal holes as opposed to a predominantly radial polarization direction in the rest of the corona. The observed emission and polarization were suggested as the signature of very fine interplanetary dust grains, i.e., it was attributed to a first signature of interplanetary dust in the form of fluorescence from silicon nanoparticle dust grains in the inner corona. It also appears at larger distances in other regions of the corona once the Fe xiii intensity has dropped significantly. Although there was no signature of neutral silicon nanoparticles exhibiting reasonably sharp fluorescence lines, the present calculations show that the ionized form of silicon nanoparticle dust grains in the inner corona has atom-like fluorescence lines because of ionizing solar UV radiation. It is plausible that one of the lines in this spectrum is responsible for the polarization observations.

In the inner corona, significant Lyman α, the fingerprint of hydrogen, is found to originate from the inner corona, followed by resonance scattering of the sun's wide-band radiation at the *L*α by entering hydrogen. In our studies, we used resonance scattering of known transitions in highly stripped or heavy ions of iron and compared it to light associated with electrons (i.e., white light) to map out local regions where there is more ion concentration than concentrations of electrons. We are applying such techniques to search for the concentration of neutrals or nanograins and their ion versions. Our measurements and simulations show that it is this resonance scattering by the hydrogen coating on the nano-Si grains that strongly deflects and hence protects the particles from the harsh Lyman α of the sun.

V. CONCLUSION

Emission showering between valence states ("Coulomb-induced" states) via hole hopping is found to be very weak because of very small oscillator strength or/and longer emission wavelength (in the infrared). Thus, de-excitation by showering is much slower than the UV/blue optical transitions (to the half-filled HOMO edge). In other words, the rate of energy loss to infra-red/heat due to Coulomb scattering is not significant. As a result, the UV/blue luminescence dominates even for excitation as high as 22 eV, the range studied in this report.

In conclusion, we demonstrated the existence of bright trion states for excitation above the ionization limit in 1 nm Si nanoparticles. In these ultrasmall particles, electron–phonon scattering is reduced, allowing a single-photon to induce a two-electron process, in which one electron is ionized and the other is simultaneously excited to a luminescent state. The trion state becomes bright because Coulomb induced states in the stripped particle have weak oscillator strength transitions and deep infrared emission frequencies, effectively diminishing or softening heat generating Coulomb scattering. The bright states are indicative of the emergence of the strong molecular-like nature of the semiconductor nanoparticle in a transition regime between the solid and molecule.

The interaction of ionizing radiation, i.e., of a single photon of energy larger than the ionization energy of the neutral, may be understood in terms of this partial energy level diagram. The figure shows three different pathways that may dominate the excitation. In the first pathway (left), an electron is excited from the top of the valence band into the ionization continuum at threshold, creating a hole in the top of the valence band (half-filled HOMO), with a second electron being excited via electron–electron correlation from lower levels in the valence band to fill the vacancy. This process is equivalent to state hopping of a single hole within the valence band. The transitions associated with the hole state hopping are due to the presence of the positive charge and as such we call them "Coulomb-induced" states. In the second pathway (center), the excess photon energy may alternatively excite an electron from the half-filled HOMO via electron–electron scattering to above gap states, which creates an exciton; hence, in the particle, there will be two holes and one electron, or what is called a positive trion state ($X+$). This is like ionized hydrogen molecule H_2^+ if $m_e << m_h$. The third pathway (right) involves direct single electron excitation from low lying states in the valence band to ionization threshold, creating a hole deep in the valence band. This process is also equivalent to single hole state hopping within the valence band. The branching ratio of the processes depends on the magnitude of the excess photon energy and the strength of the electron–electron correlation, as well as the ionization cross-sections.

AUTHOR DECLARATIONS

Conflict of Interest

The authors have no conflicts to disclose.

Author Contributions

Kevin Mantey: Data curation (equal); Formal analysis (equal); Investigation (equal); Resources (equal); Software (equal); Validation (equal); Visualization (equal); Writing – original draft (equal). **Huw Morgan**: Data curation (equal); Formal analysis (equal); Investigation (equal); Methodology (equal); Resources (equal); Validation (equal); Writing – original draft (equal). **Ammar Nayfeh**: Data curation (equal); Formal analysis (equal); Investigation (equal); Methodology (equal); Resources (equal); Software (equal); Validation (equal); Visualization (equal); Writing – original draft (equal); Writing – review & editing (equal). **Ersin Bahceci**: Data curation (equal); Formal analysis (equal); Investigation (equal); Methodology (equal); Resources (equal); Software (equal); Validation (equal); Writing – original draft (equal); Writing – review & editing (equal). **Munir H. Nayfeh**: Conceptualization (equal); Data curation (equal); Formal analysis (equal); Funding acquisition (equal); Investigation (equal); Methodology (equal); Project administration (equal); Resources (equal); Software (equal); Supervision (equal); Validation (equal); Visualization (equal); Writing – original draft (equal); Writing – review & editing (equal).

DATA AVAILABILITY

The data that support the findings of this study are available from the corresponding author upon reasonable request.

REFERENCES

[1] A. Rudenko, K. Ladutenko, S. Makarov, and T. E. Itina, Adv. Opt. Mater. **6**, 1701153 (2018).
[2] Y. Yang, W. Wang, A. Boulesbaa, I. I. Kravchenko, D. P. Briggs, A. Puretzky, D. Geohegan, and J. Valentine, Nano Lett. **15**, 7388 (2015).
[3] G. Della Valle, B. Hopkins, L. Ganzer, T. Stoll, M. Rahmani, S. Longhi, Y. S. Kivshar, C. De Angelis, D. N. Neshev, and G. Cerullo, ACS Photonics **4**, 2129 (2017).
[4] S. V. Makarov, A. S. Zalogina, M. Tajik, D. A. Zuev, M. V. Rybin, A. A. Kuchmizhak, S. Juodkazis, and Y. Kivshar, Laser Photonics Rev. **11**, 1700108 (2017).
[5] P. P. Iyer, N. A. Butakov, and J. A. Schuller, ACS Photonics **2**, 1077 (2015).
[6] S. Makarov, S. Kudryashov, I. Mukhin, A. Mozharov, V. Milichko, A. Krasnok, and P. Belov, Nano Lett. **15**, 6187 (2015).
[7] M. R. Shcherbakov, P. P. Vabishchevich, A. S. Shorokhov, K. E. Chong, D.-Y. Choi, I. Staude, A. E. Miroshnichenko, D. N. Neshev, A. A. Fedyanin, and Y. S. Kivshar, Nano Lett. **15**, 6985 (2015).
[8] D. G. Baranov, S. V. Makarov, V. A. Milichko, S. I. Kudryashov, A. E. Krasnok, and P. A. Belov, ACS Photonics **3**, 1546 (2016).
[9] D. G. Baranov, S. V. Makarov, A. E. Krasnok, P. A. Belov, and A. Alù, Laser Photonics Rev. **10**, 1009 (2016).
[10] M. R. Shcherbakov, S. Liu, V. V. Zubyuk, A. Vaskin, P. P. Vabishchevich, G. Keeler, T. Pertsch, T. V. Dolgova, I. Staude, I. Brener, and A. A. Fedyanin, Nat. Commun. **8**, 1 (2017).
[11] J. Leuthold, C. Koos, and W. Freude, Nat. Photonics **4**, 535 (2010).
[12] D. P. Korfiatis, K.-A. T. Thoma, and J. C. Vardaxoglou, J. Phys. D: Appl. Phys. **40**, 6803 (2007).
[13] A. Rudenko, J.-P. Colombier, and T. E. Itina, Int. J. Numer. Modell. **31**, e2215 (2016).
[14] K. Mantey, L. Quagliano, A. Rezk, S. Palleschi, L. Abuhassan, A. Nayfeh, E. Bahceci, and M. H. Nayfeh, AIP Adv. **11**, 105206 (2021).
[15] D. D. Hickstein, F. Dollar, J. L. Ellis, K. J. Schnitzenbaumer, K. E. Keister, G. M. Petrov, C. Ding, B. B. Palm, J. A. Gaffney, M. E. Foord, S. B. Libby, G. Dukovic, J. L. Jimenez, H. C. Kapteyn, M. M. Murnane, and W. Xiong, ACS Nano **8**, 8810 (2014).
[16] H. M. van Driel, Phys. Rev. B **35**, 8166 (1987).
[17] G. Mie, Ann. Phys. **330**, 377 (1908).
[18] S. Jahani and Z. Jacob, Nat. Nanotechnol. **11**, 23 (2016).
[19] A. I. Kuznetsov, A. E. Miroshnichenko, M. L. Brongersma, S. Y. Kivshar, and B. Luk'yanchuk, Science **354**, aag2472 (2016).
[20] T. J.-Y. Derrien, T. E. Itina, R. Torres, T. Sarnet, and M. Sentis, J. Appl. Phys. **114**, 083104 (2013).
[21] M. H. Nayfeh , O. Akcakir, G. Belomoin, N. Barry, J. Therrien, and E. Gratton, Appl. Phys. Lett. **77**, 4086 (2000).
[22] M. W. Schmidt, K. K. Baldridge, J. A. Boatz, S. T. Elbert, M. S. Gordon, J. H. Jensen, S. Koseki, N. Matsunaga, K. A. Nguyen, S. Su, T. L. Windus, M. Dupuis, and J. A. Montgomery, J. Comput. Chem. **14**, 1347 (1993).
[23] M. S. Gordon and M. W. Schmidt, *Advances in Electronic Structure Theory: GAMESS a Decade Later* (Elsevier, Amsterdam, 2005).
[24] See the website of the Mark Gordon group http://www.msg.ameslab.gov/gamess/gamess.html for information about theory development and application of quantum chemical methods to interesting problems including the GAMESS teamwork towards the Exa-scale Computing Project.
[25] K. Mantey, A. Zhu, J. Boparai, M. Nayfeh, C. Marsh, and G. Al Chaar, Phys. Rev. B **85**, 085417 (2012).
[26] J. Malloy, K. Mantey, Y. Maximenko, E. Bahceci, H. Morgan, Z. Yamani, J. Boparai, K. Puthalath, and M. H. Nayfeh, J. Appl. Phys. **124**, 044501 (2018).
[27] M. A. Lampert, Phys. Rev. Lett. **1**(12), 450 (1958).
[28] P. K. Samanta, Phys. AUC **28**, 17 (2018).
[29] S. Rao, K. Mantey, J. Therrien, A. Smith, and M. Nayfeh, Phys. Rev. B **76**, 155316 (2007).
[30] Z. Yamani, W. H. Thompson, L. AbuHassan, and M. H. Nayfeh, Appl. Phys. Lett. **70**, 3404 (1997).
[31] O. Ackakir, J. Therrien, G. Belomoin, N. Barry, J. Muller, E. Gratton, and M. Nayfeh, Appl. Phys. Lett. **76**, 1857 (2000).
[32] M. H. Nayfeh, E. V. Rogozhina, and L. Mitas, "Silicon nanoparticles: Next generation of ultrasensitive fluorescent markers," in *Synthesis, Functionalization, and Surface Treatment of Nanoparticles*, edited by M.-I. Baraton (American Scientific Publishers, 2002).
[33] M. H. Nayfeh, L. Mitas, and V. Kumar, *Silicon Nanoparticles. New Photonic and Electronic Material at the Transition between Solid and Molecule* (Elsevier, 2007).
[34] M. H. Nayfeh, *Fundamentals and Applications of Nano Silicon in Plasmonics and Fullerenes: Current and Future Trends* (Elsevier Publishing, 2018).
[35] G. Belomoin, J. Therrien, A. Smith, S. Rao, R. Twesten, S. Chaieb, M. H. Nayfeh, L. Wagner, and L. Mitas, Appl. Phys. Lett. **80**, 841 (2002).
[36] D. Nielsen, L. Abuhassan, M. Alchihabi, A. Al-Muhanna, J. Host, and M. H. Nayfeh, J. Appl. Phys. **101**, 114302 (2007).
[37] K. Mantey, H. Morgan, J. Boparai, Z. Yamani, E. Bahceci, and M. H. Nayfeh, AIP Adv. **11**, 095319 (2021).
[38] N. Elhalawany, Y. Maximenko, Z. Yamani, S.-T. Yau, and M. H. Nayfeh, Mater. Res. **28**, 2 (2013).
[39] Y. Chao, A. Houlton, B. R. Horrocks, M. R. C. Hunt, N. R. J. Poolton, J. Yang, and L. Šiller, Appl. Phys. Lett. **88**, 263119 (2006).
[40] S. Rao, J. Sutin, R. Clegg, E. Gratton, M. H. Nayfeh, S. Habbal, A. Tsolakidis, and R. M. Martin, Phys. Rev. B **69**, 205319 (2004).
[41] L. Mitas, J. Therrien, R. Twesten, G. Belomoin, and M. H. Nayfeh, Appl. Phys. Lett. **78**, 1918 (2001).
[42] G. Allan, C. Delerue, and M. Lannoo, Phys. Rev. Lett. **76**, 2961 (1996).
[43] E. W. Draeger, J. C. Grossman, A. J. Williamson, and G. Galli, Phys. Rev. Lett. **90**, 167402 (2003).
[44] D. Sundholm, Nanolett. **3**, 847 (2003).
[45] O. Lehtonen and S. Sundholm, Phys. Rev. B **72**, 085424 (2005).
[46] D. V. Melnikov and J. R. Chelikowsky, Phys. Rev. B **69**, 113305 (2004).
[47] J. V. Ortiz, J. Chem. Phys. **94**, 6064 (1991).
[48] Z. H. Yamani, "Optical properties of size selected nanocrystallites in porous silicon," University of Illinois at Urbana-Champaign ProQuest Dissertations Publishing (1999), Vol. 1999, p. 9953180.
[49] S. K. Rao, K. Mantey, J. Therrien, A. Smith, and M. Nayfeh, "A study of the molecular behavior in the vibronic and excitonic properties of silicon nanoparticles," Ph. D. Thesis, University of Illinois at Urbana-Champaign, Champaign, IL, 2006.
[50] A. Tanaka, N. Takashima, M. Imamura, T. Kitagawa, Y. Murase, and H. Yasuda, J. Phys. Soc. Jpn. **77**, 094701 (2008).
[51] S. R. Habbal, M. B. Arndt, M. H. Nayfeh, J. Arnaud, J. Johnson, S. Hegwer, R. Woo, A. Ene, and F. Habbal, Astrophys. J. **592**, L87 (2003).
[52] M. H. Nayfeh, *Total Eclipse* (International Innovation, UK, 2012), p. 90.
[53] M. H. Nayfeh, S. R. Habbal, and S. Rao, Astrophys. J. **621**, L121 (2005).
[54] R. Woo and S. R. Habbal, Geophys. Res. Lett. **24**, 1159, https://doi.org/10.1029/97gl01156 (1997).